Simulation and experimental study of the thermal characteristics of a high-speed motorized spindle

Wei Zhang[1,2*], Huaqiao Jiang[2]

[1]China Light Industry Plastic Mold Engineering Technology Research Center, Ningbo Polytechnic, Ningbo 315800, China
[2]Ningbo Shuaitelong Group Co., Ltd, Ningbo 315000, China
*Corresponding author email: zw111150@163.com

Abstract

Based on the finite element simulation software ANSYS Workbench, this study reports the thermal characteristics of a high-speed motorized spindle. The temperature field distribution and axial thermal deformation of the motorized spindle are then detected on an experimental platform. A comparison between the experimental and simulation results revealed the temperature rise of the motorized spindle during the working process. Under steady-state conditions of the working motorized spindle, the temperatures of the front bearing, rear bearing and stator were determined as 20°C, approximately 30°C and 25°C, respectively. The axial thermal elongation of the motorized spindle is approximately 10 μm.

1. Introduction

The electric spindle is the core component of high-speed machine tools. A high-speed electric spindle is highly integrated and has a compact internal structure that impedes heat dissipation from the bearings and motors. Consequent thermal deformation of the electric spindle considerably reduces the machining accuracy, production efficiency and service life of the machine tool. As thermal errors can account for up to 70% of the total error of the machine tool [1–3], thermal problems have dominated research on high-speed electric spindles. Zhang et al. studied a coupled model of thermal-flow-structure. The simulation results showed that when the diameter of the cooling channel is 7 mm, a spiral cooling system develops a lower temperature but greater radial thermal deformation than a U-shaped cooling system [4]. Su et al. established a thermal fluid-solid coupling model of a hydrostatic spindle system using the finite volume method. They simulated the heat generation of the heat source and the fluid-solid heat transfer process [5]. Other researchers analyzed the internal friction force and established a friction dynamics model of the bearing [6, 7]. It was found that sliding friction movement between the bearing ball and the rolling element intensifies after increasing the bearing speed and lowering the preload. Chen et al. [8] studied the influence of rotational speed on the temperature field distribution of a high-speed electric spindle. They reported a linear temperature rise of the electric spindle from 6 000 to 10 000 rpm. At speeds exceeding 10 000 rpm, the temperature rise became exponential owing

to the intense heat generated by friction between the front and rear bearings. The method of Kumar et al. [9] selects the optimal number of temperature sensors for predicting the thermal deformation at the required prediction accuracy. The model accuracy was 86.72% with two temperature sensors and 85.99% with one temperature sensor. They concluded that a single temperature sensor can sufficiently predict the deflection of the tool centre point with an accuracy compromise of 0.73%.

Applying the finite element method in ANSYS Workbench, the present authors simulate and study the thermal characteristics of an electric spindle. The simulation results are experimentally verified by measuring the temperature field distribution and axial thermal deformation of the electric spindle. This paper reveals the temperature rise during the working process of the electric spindle, along with the temperature field distribution and axial thermal deformation of the electric spindle under thermally stable conditions, providing a reference and guidance for the thermal design of electric spindles.

2. Materials and research methods

2.1. Simulation model and grid division

The structural models of electric spindles in practical engineering applications are commonly complex. Finite element analyses of the original model require a large number of calculations, which are difficult to run and often obtain non-ideal results. To avoid these problems, a reasonable finite element model for a specific problem must be developed before running the finite element analysis. The present study adopts a series of simplified methods for electric spindle modelling. Smooth component surfaces are assumed and the chamfers, fillets, threaded holes, and small protrusions on the original model are assumed to negligibly affect the thermal structure analysis. Factors with low impact on the thermal analysis, such as the broach in the model and the spiral flow channel on the shell, are also neglected. The surfaces of irregular parts, such as the balls in ball bearings, are simplified as circular rings with the dimension of rolling diameter. The proposed dynamic model is developed based on a high-speed end milling spindle (Model: CFV12000) of rated power 7.5 kW with a maximum spindle speed of 12 000 rpm, an installation dimension of 180 mm and a front bearing diameter of 70 mm. A cross-section of the simplified model is shown in Fig. 1. ANSYS includes various meshing methods for three-dimensional

geometries, such as Automatic, Tetrahedral, and Sweep Meshing. The present simulation uses the sweeping method for grid division. The results of the grid division are shown in Fig. 1. The grid size is set to 4 mm and the final number of divided nodes is 291 869 with 147 785 units.

The centre spindle and broach bar of the electric spindle are composed of 20CrMnTi, the spacer parts are composed of GB-standard alloy bearing steel (GCr15), and all other parts are composed of 40Cr. 20CrMnTi, GCr15, and 40Cr were added as new materials to the material library of ANSYS Workbench, and their densities, Young's moduli and Poisson's ratio were assigned to the values given in Table 1.
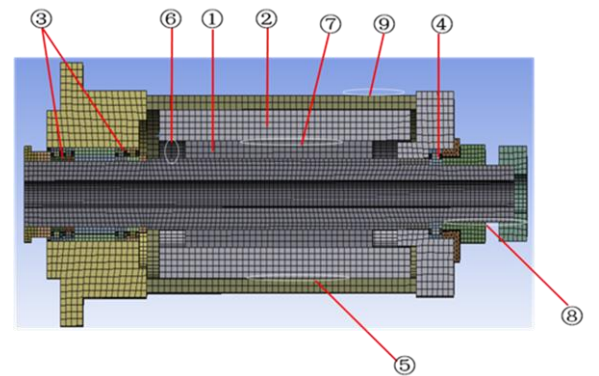
Fig. 1. Cross-section and grid division
of the electric spindle model.

2.2. Calculation of thermal boundary conditions

Before analyzing the thermal characteristics of an electric spindle using the finite element method, we must determine the boundary conditions. In the present study, boundary conditions are required only for the heat source and convective heat transfer.

2.2.1. Calculation of heat generation rate of heat source

An electric spindle is heated mainly by losses of the stator and rotor, including magnetic loss, electrical loss and friction loss. The rated heat output Q of a motor is calculated as

Table 1. Properties of the electric spindle materials.

Material	Density (kg/m³)	Elastic modulus (GPa)	Poisson's ratio	Thermal expansion coefficient (K-1)	Specific heat capacity (J/(kg.K))	Thermal conductivity (W/(m.K))
GCr15	7810	219	0.300	1.4e-5	553	40.11
40Cr	7870	211	0.277	1.2e-5	460	34.00
20CrMnTi	7860	212	0.289	1.3e-5	460	44.00
GCr15	7810	219	0.300	1.4e-5	553	40.11

$$Q = P\frac{(1-\eta)}{\eta}, \tag{1}$$

where P is the rated output power of the motor and η is the motor efficiency

The thermal characteristics of the feed system largely depend on the friction heat generated in the rolling bearings, which is mainly caused by friction torque on the bearings and the viscous friction of the lubricants. Palmgren obtained an empirical formula for the friction torque on rolling bearings [10]. The heat flow H in the bearings is the following function of friction torque and speed:

$$H = M \times n_z \times 1.047 \times 10^{-4}, \tag{2}$$

$$M = M_1 + M_v. \tag{3}$$

In this formula, M is the total friction torque on the bearings, (N·mm), n_z is the bearing speed (rpm), and M_1 is the friction loss related to the bearing load which reflects elastic hysteresis and local sliding. M_v is the speed-related fluid power loss in the reaction lubricant.

2.2.2. Calculation of convective heat transfer coefficient

The convective heat transfer coefficient mainly depends on the cooling of the main shaft by circulating cooling oil and the other surface convective coefficients of the main shaft. As the cooling oil flows through a spiral cooling groove, it extracts the heat transferred from the main shaft. The heat is exchanged through the oil–water exchange system and the oil returns to the oil tank for the next cycle. The convective heat transfer coefficient α_1 was calculated using the Nusselt equation [11] under forced convection conditions:

$$\alpha_1 = \frac{\mathrm{Nu}\lambda}{d}, \tag{4}$$

where Nu is the Nusselt number, λ is the thermal conductivity of the fluid and d is the diameter of the conducting cylindrical surface.

In practical applications, the heat transfer through pipes is usually turbulent. The Nusselt number of turbulent heat transfer is calculated using the Dittus–Boelter formula [12] as

$$\mathrm{Nu} = 0.023\mathrm{Re}^{0.8}\mathrm{Pr}^N , \tag{5}$$

for $\mathrm{Re} > 1\,000, 0.7 < \mathrm{Pr} < 120$.

In Eq. (5), Re is the Reynolds number and Pr is the Prandtl number. $N = 0.4$ when heating the fluid and 0.3 when cooling

the fluid. L/d is the ratio of pipe length to pipe diameter during internal convection. By introducing the Nu value to the convective heat transfer formula, we can calculate the forced convective heat transfer coefficient between the coolant and the spindle sleeve.

The convective coefficients on the other surfaces of the axis determine whether the fluid flow is laminar or turbulent [13]. The empirical formula for selecting Nu is based on the flow pattern. The values of Pr and λ depend on the fluid properties. Finally, the convective heat transfer coefficient is calculated using Eq. (4).

Table 2. Calculated heat generation rates and heat transfer coefficients for the main components of the electric spindle.

Fig. 1	Parameter	Calculation results
1	Heat generation rate of motor stator q_d (W/m³)	2.00×10⁵
2	Heat generation rate of motor rotor q_z (W/m³)	4.00×10⁵
3	Heat generation rate of front bearing q_f (W/m³)	4.00×10⁵
4	Heat generation rate of rear bearing q_r (W/m³)	3.00×10⁶
5	Convective heat transfer coefficient between cooling oil and electric spindle α (W/(m²K))	850.00
6	Convective heat transfer coefficient between the rotor end and surrounding air α_{t1} (W/(m²K))	172
7	Coefficient of convective heat transfer between stator and rotor gaps α_{t2} (W/(m²K))	146
8	Convective heat transfer coefficient of other moving surfaces of the spindle α_{t3}(W/(m²K))	180
9	Convective heat transfer coefficient on other stationary surfaces of the main shaft α_{t4} (W/(m²K))	9.70

2.2.3. Calculated heat generation rate and convective heat transfer coefficient of the heat source

The estimates of some components found from empirical formulas may be inaccurate and deviate from the actual values. Therefore, some data were adjusted to fit the actual situation during the simulation. Table 2 lists the adjusted heat generation rates and heat transfer coefficients of the main components, which were loaded into the ANSYS Workbench for analysis.

Typical electric spindles used in practical engineering are complex assemblies of solid components. To ensure heat transfer between these components, the contact area between the entities is automatically created. Heat transfer occurs only between two parts that are initially in contact. The junction surface is set as a bond connection. According to [14], the heat transfer coefficient of each junction surface of a motorized spindle is 3 200 W/(m²·K).

2.3 Experimental study on the thermal characteristics of three electric spindles

The thermal characteristics of electric spindles must be experimentally determined because finite element simulations inevitably contain numerical errors. Combining experimental methods with finite element analyses can improve the accuracy of thermal characterization of electric spindles. The thermal drift at the end of the spindle and the thermal tilt of the spindle were measured using the 5-point method (sensors installation points x_1, x_2, y_1, y_2, and z in Fig. 2). To measure the temperature field and axial thermal deformation of the electric spindle, this study adopts displacement measurement systems with the appropriate measurement range, resolution, thermal stability and accuracy, along with high-precision capacitive sensors and a thermal-resistance temperature sensor with sufficient resolution and accuracy (LION PT100 with class A accuracy, a measurement error of $\pm[0.15°C + 0.002|t|]$ and measurement range of $-50°C–500°C$). The thermal-resistance temperature sensor was placed in a pre-drilled hole inside the spindle and the sensors were installed at three positions: the front bearing outer ring, the rear bearing outer ring and the rotor. Data were acquired by a dial indicator that detects the reference movement distance of the electric spindle. The dial indicator should meet the corresponding standards and be provided by relevant suppliers or enterprises. These gauges (accuracy class 0; measurement error ±0.002) were installed on the machine tool as shown in Fig. 2.

The steps for conducting thermal characteristic experiments are as follows: The experimental device was thoroughly cleaned to remove dirt from the device platform, which interferes with the results of the high-accuracy capacitive displacement sensors and inspection rods (resolution 0.06 nm; adjustable bandwidth up to 15 kHz). Next, the inspection instruments and tools were installed in a certain order. All necessary levelling, geometric adjustments and functional inspections of the equipment should be completed prior to the experiment, and the initial experimental conditions must be confirmed and recorded. The initial temperature, front- and rear bearing temperature, stator temperature, and cooling oil flow of the thermal characterization were set to 17.35°C, 18.6°C, 24°C and 24 l/min, respectively. In preparation for the experiments, the machine tool was preheated at 6 000 rpm for five minutes. During the experiments, the speed was increased to 12 000 rpm and continued for approximately two hours while the data were recorded in real time. Recorded were the temperatures of the front and rear bearings, the temperature of the cooling oil, the displacement degree of the sensor and the temperature of the stator. During the first 30 minutes, the experimental data were recorded at half-minute intervals because the temperature of the electric spindle rapidly changed

over this period. From 30 minutes to one hour, the overall temperature trend of the electric spindle slowed so the recording period was increased to one minute. After one hour, when the overall temperature of the electric spindle had stabilized, the recording period was further extended to three minutes.

3. Results and analysis

3.1. Simulation results and analysis

3.1.1. Temperature field analysis

Figure 3 shows the simulated temperature field of the electric spindle. The steady-state temperatures of the front bearing, rear bearing, stator and rotor were approximately 20°C, 31°C, 25°C and 35°C, respectively. The temperature field reveals the components with large heat capacity and the key heating areas (rotor and rear bearing). Accurate determination of the heat capacity is crucial for accurate thermal analysis of the motorized spindle. The temperature field analysis of the motorized spindle preliminarily determines the effectiveness of a thermal design and indicates the direction of thermal structure optimization. First, the
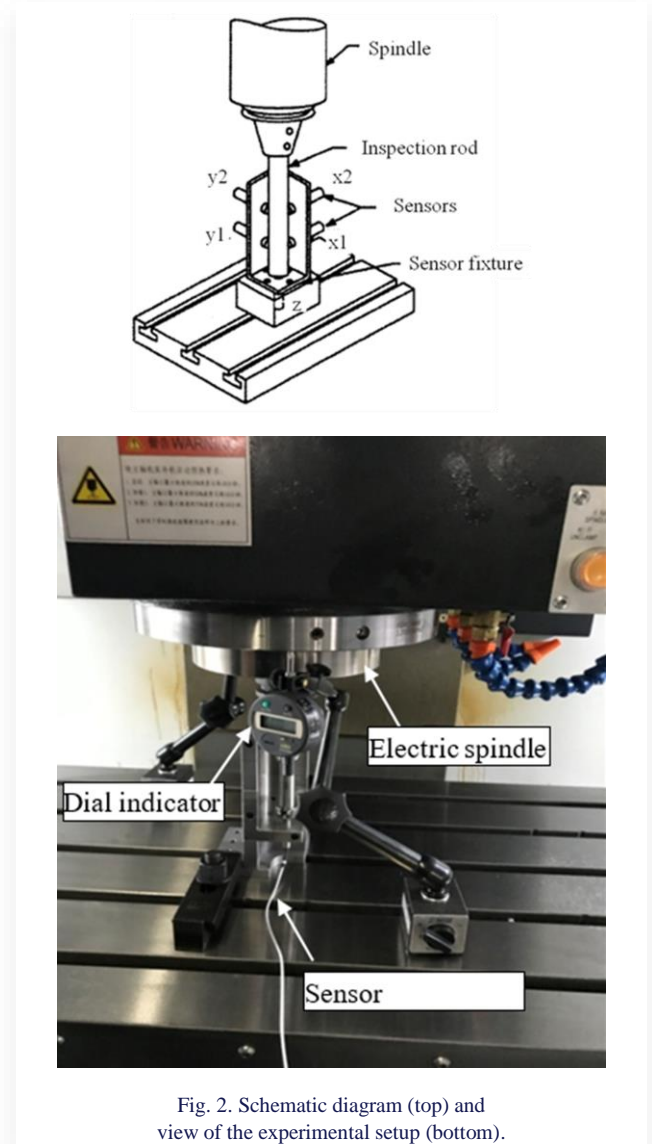
Fig. 2. Schematic diagram (top) and
view of the experimental setup (bottom).

key components with large thermal capacity can be optimized to control the heating of the motorized spindle. Second, the heat sources can be symmetrically distributed to prevent thermal tilting and reduce harmful thermal deformation. Third, a thermal equilibrium design of the motorized spindle structure will ensure an evenly distributed temperature field. Finally, the motorized spindle is guided to expand and contract regularly in the desired direction with the desired displacement, laying the foundation of reasonable thermal control.
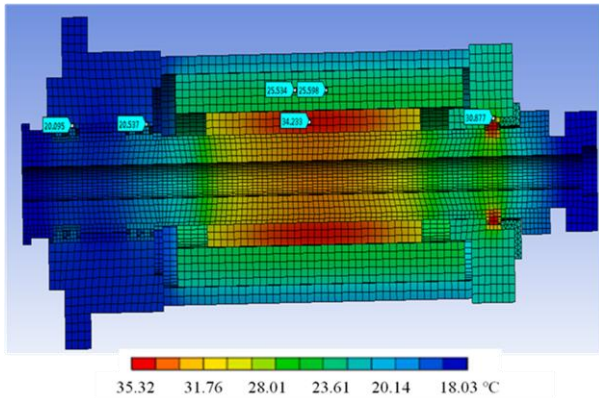
Fig. 3. Calculated temperature field of the electric spindle
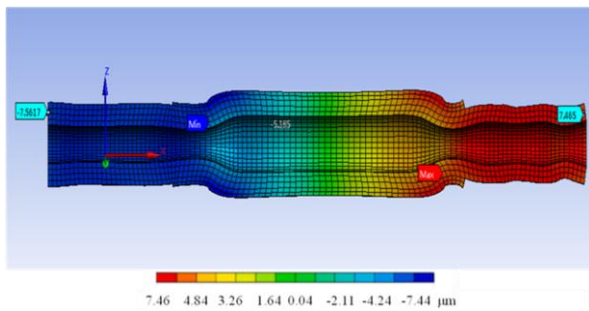
Fig. 4. Calculated axial thermal elongation of the electric spindle.

3.1.2. Thermal deformation analysis

Figure 4 shows the calculated axial thermal elongation of the electric spindle. The maximum thermal elongation appears in the middle of the electric spindle. The front and rear ends are elongated by approximately 7.5 μm. The maximum axial deformation is located at the rear end of the main spindle, because heat is transmitted from the high temperature area to the low temperature area. The final axial deformation will be most obvious at the lowest temperature area because of heat conduction. As the temperature at the rear end of the main shaft is the lowest temperature area of the entire main spindle, the thermal deformation is the largest. When thermally designing an electric spindle, one must first consider the deformation amounts of the most severely deformed components along the axial direction. Therefore, a structural thermal equilibrium design of the key components is necessary for obtaining the overall thermal deformation of the motorized spindle and hence achieving an overall optimized design with a balanced and symmetric structure.

3.2. Experimental results and analysis

3.2.1. Experimentally determined temperature field

Figure 5 plots the time courses of temperatures in different parts of the electric spindle. Between startup and steady-state, the temperatures of the front and rear bearings rose by approximately 1°C (steady-state temperature 20°C) and 10°C (steady-state temperature 28.5°C), respectively. The temperatures of the stator and cooling oil inlet temperature remained nearly constant, stabilizing at 25°C and 17.5°C, respectively. The measured values were very close to the simulation results, in which the approximate steady-state temperatures of the front bearing, rear bearing and stator were 20°C, 31°C and 25°C, respectively. Therefore, the rotor is the main heat source of the motorized spindle during operation. When thermally designing a motorized spindle, ensuring thermal equilibrium of the heat source and designing a reasonably motorized spindle structure are essential.

3.2.2. Experimentally determined thermal deformation

Figure 6 plots the axial thermal elongation of the electric spindle versus time. Here, the axial thermal elongation alone was tested because it substantially influenced the performance of the machining tool. During the experiment, the axial thermal elongation of the electric spindle remained stable at 10.5 μm after 40–60 minutes and slowly decreased as the room temperature
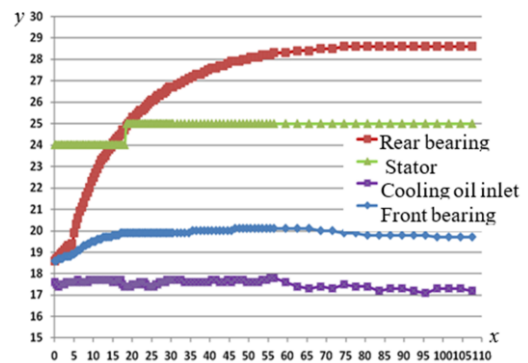
Fig. 5. Measured axial thermal elongation of the electric spindle (y coordinate: thermal elongation (um); x coordinate: time (min))
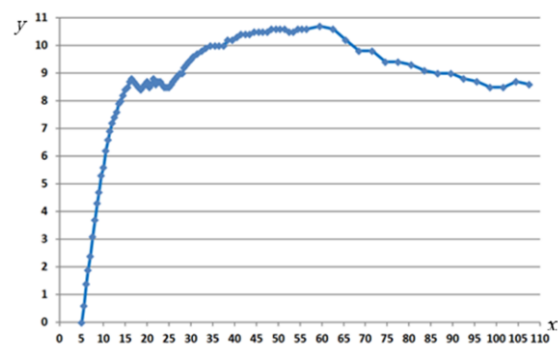
Fig. 6. Measured temperatures of the electric spindle components (y coordinate: temperature (°C); x coordinate: time (min)).

decreased in the later stages of the experiment. The stable elongation (10.5 μm) was regarded as the maximum thermal elongation of the electric spindle. The simulated thermal elongation of the electric spindle (7.5 μm) agreed with the experimental result within the allowable error range [15, 16]. Therefore, we speculate that the thermal elongation of the electric spindle is between 8 and 10 μm. The impact of the whole thermal elongation must be considered when designing an electric spindle. If the inferred thermal elongation exceeds the requirements, the spindle must be redesigned while considering (1) whether thermal symmetry is required, (2) whether an even temperature field distribution is required, and (3) whether the cooling conditions should be strengthened.

4. Conclusions

This article investigated the thermal characteristics of a high-speed motorized spindle through finite element simulations using the ANSYS Workbench software. First, the thermal characteristics of the electric spindle were simulated and the simulation results were experimentally verified. The results revealed that the temperature rises during the working process of the electric spindle. The temperature field distribution and axial thermal deformation of the electric spindle were determined under thermally stable conditions. The main conclusions are summarized below.

At an initial room temperature and cooling oil-flow rate of 17.35°C and 24 l/min, respectively, the motorized spindle operated at 12 000 rpm. During stable-state operation, the front bearing temperature, rear bearing temperature and stator temperature were approximately 20°C, 30°C and 25°C, respectively. Under axial thermal expansion, the electric spindle was elongated by approximately 10 μm. The experimental and simulation results deviated within the allowable error range. We inferred that the actual thermal elongation of the electric spindle is between 8 and 10 μm. Meanwhile, the main heat sources of the operating electric spindle are the rear bearing and rotor. When designing the electric spindle, one must fully consider the thermal balance of the heat source and the structure of the electric spindle. These results provide a reference and guidance for the thermal design of electric spindles.

References

[1] Hao, J., Li, C.Y., Song, W.J., Yao, Z.H., Miao, H.H., Xu, M.T., et al. (2023). Thermal-mechanical dynamic interaction in high-speed motorized spindle considering nonlinear vibration. *International Journal of Mechanical Sciences*, 240(2), 107959. doi: 10.1016/J.IJMECSCI.2022.107959

[2] Dai, Y., Tao, X.S., Xuan, L.Y., Ou, H., & Wang, G. (2022). Thermal error prediction model of a motorized spindle considering variable preload. *The International Journal of Advanced Manufacturing Technology*, 121(7–8), 4745–4756. doi: 10.1007/S00170-022-09679-Y

[3] Dai, Y., Tao, X.S., Li, Z.L., Zhan, S.Q., Li, Y., & Gao, Y.H. (2022). A Review of Key Technologies for High-Speed Motorized Spindles of CNC Machine Tools. *Machines*, 10(2), 145. doi: 10.3390/MACHINES10020145

[4] Zhang, Y., Wang, L.F., Zhang, Y.D., & Zhang, Y.D. (2021). Design and thermal characteristic analysis of motorized spindle cooling system. *Advances in Mechanical Engineering*, 13(5), 781–802. doi: 10.1177/16878140211020878

[5] Su, H., Lu, L.H., Liang, Y.C., Zhang, Q., Sun, Y. (2014). Thermal analysis of the hydrostatic spindle system by the finite volume element method. *The International Journal of Advanced Manufacturing Technology*, 71(9–12), 1949–1959. doi: 10.1007/s00170-014-5627-8

[6] Sun, X. Y. (2019). *Investigation on Thermal Characteristics and Cooling Method for High-speed Motorized Spindle*. Shanghai Jiaotong University. doi: 10.27307/d.cnki.gsjtu.2019.002077

[7] Su, C., & Chen, W. (2022). An optimized thermal network model to evaluate the thermal behavior on motorized spindle considering lubricating oil and contact factors. *Proceedings of the Institution of Mechanical Engineers, Part C: Journal of Mechanical Engineering Science*, 236(13), 7484–7499. doi: 10.1177/09544062221075171

[8] Zhang, C.X., Chen, L.F., Wang, W.M., & Liu, F.L. (2015). Research on high-speed motorized spindle thermal characteristics: simulation and experiment. *Journal of Beijing University of Chemical Technology (Natural Science Edition)*, 42(6), 90–96. doi: 10.13543/j.cnki.bhxbzr.2015.06.015

[9] Kumar, S., & Srinivasu, D.S. (2022). Optimal number of thermal hotspots selection on motorized milling spindle to predict its thermal deformation. *Materials Today: Proceedings*, 62(6), 3376–3385. doi: 10.1016/J.MATPR.2022.04.267

[10] Sun, S., Qiao, Y., Gao, Z., Wang, J., & Bian, Y. (2023). A thermal error prediction model of the motorized spindles based on AB-HHO-LSSVM. *The International Journal of Advanced Manufacturing Technology*, 127(5–6), 2257–2271. doi: 10.1007/S00170-023-11429-7

[11] Truong, D.S., Kim, B.S., & Ro, S.K. (2021). An analysis of a thermally affected high-speed spindle with angular contact ball bearings. *Tribology International*, 157(5), 106881. doi: 10.1016/J.TRIBOINT.2021.106881

[12] Kumar, B.V., Manikandan, G., & Kanna, P.R. (2021). Enhancement of heat transfer in SAH with polygonal and trapezoidal shape of the rib using CFD. *Energy*, 234(9), 121154. doi: 10.1016/ j.energy.2021.121154

[13] Singh, A., & Singh, D.K. (2021). An investigation on the forced convection heat transfer in the gap of two rotating disks with laminar inflow. *Heat Transfer*, 50(7), 6964–6983. doi: 10.1002/htj.22212

[14] Tang, Y., Jing, X., Li, W., He, Y., & Yao, J.X. (2021). Analysis of influence of different convex structures on cooling effect of rectangular water channel of motorized spindle. *Applied Thermal Engineering*, 198(5), 117478. doi: 10.1002/htj.22212

[15] Jiang, Z.Y., Huang, X.Z., Chang, M.X., Li, C., & Ge, Y. (2021). Thermal error prediction and reliability sensitivity analysis of motorized spindle based on Kriging model. *Engineering Failure Analysis*, 127(9), 105558. doi: 10.1016/J.ENGFAILANAL.2021.105558

[16] Cheng, Y., Zhang, X., Zhang, G., Jiang, W., & Li, B. (2022). Thermal error analysis and modeling for high-speed motorized spindles based on LSTM-CNN. *The International Journal of Advanced Manufacturing Technology*, 121(5/6), 3243–3257. doi: 10.1007/S00170-022-09563-9